Supplement of Atmos. Chem. Phys., 25, 1725–1748, 2025
https://doi.org/10.5194/acp-25-1725-2025-supplement

Atmospheric Chemistry and Physics
Open Access
EGU

Supplement of

Quantification of regional net CO_2 flux errors in the Orbiting Carbon Observatory-2 (OCO-2) v10 model intercomparison project (MIP) ensemble using airborne measurements

Jeongmin Yun et al.

Correspondence to: Jeongmin Yun (jeongmin.yun@jpl.nasa.gov) and Junjie Liu (junjie.liu@jpl.nasa.gov)

This PDF file includes:

S1. Validation of representation error estimates

Tables S1

Figures S1 to S12

S1. Validation of representation error estimates

ACT-America project provides extensive atmospheric CO_2 data across central and eastern North America spanning nine months for the period 2016–2019 (Baier et al., 2020; Wei et al., 2021). Using this observation data, we validate whether our representation errors, derived from simulated atmospheric CO_2 fields with 0.5ºx0.625º resolution, reasonably represent the actual representation errors. Airborne observations do not provide simultaneous spatial distribution information of CO_2, unlike models. Thus, we calculated the variances of observed CO_2 concentrations within each 1°x1° grid cell with a 500 m vertical interval (from 1 to 5 km) at 3-hour intervals ($OBS\_ERR_{REP}^2$). On average, each grid box includes around 70 aircraft observation data. For comparison with the $OBS\_ERR_{REP}^2$, we sampled VAR_{CO_2}, derived from GEOS-5 results, at the corresponding aircraft measurement times and locations at each grid box and computed their mean values ($MOD\_ERR_{REP}^2$). Monthly and regional mean OBS_ERR_{REP} and MOD_ERR_{REP} over North America show a significant positive correlation (r= 0.72, p <0.05) for the ACT-America project period (Figure S1). MOD_ERR_{REP} also has a similar mean value (0.62 [0.59, 0.64] ppm) with that of OBS_ERR_{REP} (0.49 [0.47, 0.51] ppm). This result supports that ERR_{REP} could reasonably represent the actual mean representation error at a 1-degree grid cell.

Table S1. Description for each OCO-2 v10 MIP inverse model. The information is from Byrne et al. (2023).

Simulation name	Transport model	Meteorology forcing		Prior terrestrial CO_2 flux	Prior air-sea CO_2 flux	Inverse method
		name	resolution			
Ames	GEOS-Chem	MERRA-2	4° × 5°	CASA-GFED4.1s	CT2019OI	4D-Var
Baker	PCTM	MERRA-2	1° × 1.25° prior, 4° × 5° opt	CASA-GFED3	Landschützer v4.4	4D-Var
CAMS	LMDz	ERA5	1.9° × 3.75°	ORCHIDEE (climatological)	CMEMS	Variational
CMS-Flux	GEOS-Chem	MERRA-2	4° × 5°	CARDAMOM	MOM-6	4D-Var
COLA	GEOS-Chem	MERRA-2	4° × 5°	VEGAS	Rödenbeck 2021	EnKF
CT	TM5	ERA5	2° × 3°/1° × 1°	CT2019 CASA GFED4.1s	CT2019OI	EnKF
OU	TM5	ERA-Interim	4° × 6°	CASA-GFED3	Takahashi	4D-Var
TM5-4DVar	TM5	ERA-Interim	2° × 3°	SiB-CASA	CT2019 Opt Clim	4D-Var
UT	GEOS-Chem	GEOS-FP	4° × 5°	BEPS	Takahashi	4D-Var
WOMBAT	GEOS-Chem	MERRA-2	2° × 2.5°	SiB-4 w/MERRA-2	Landschutzer 2020	Synthesis with MCMC

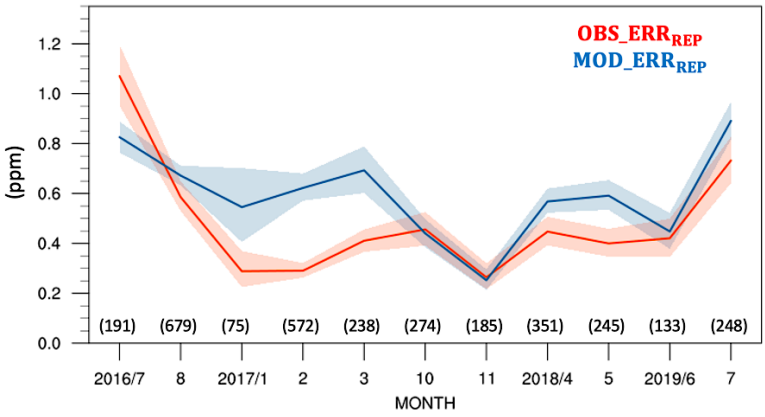

Figure S1 Monthly variations of OBS_ERR_{REP} and MOD_ERR_{REP} in the central and eastern North America for ACT-America project period during 2016–2019. The lines and shaded areas represent the mean and the 95% confidence intervals derived from 1000 bootstrap samples of the 1-degree grid-based monthly error quantities. The bottom numbers indicate the number of grid data points for each month.

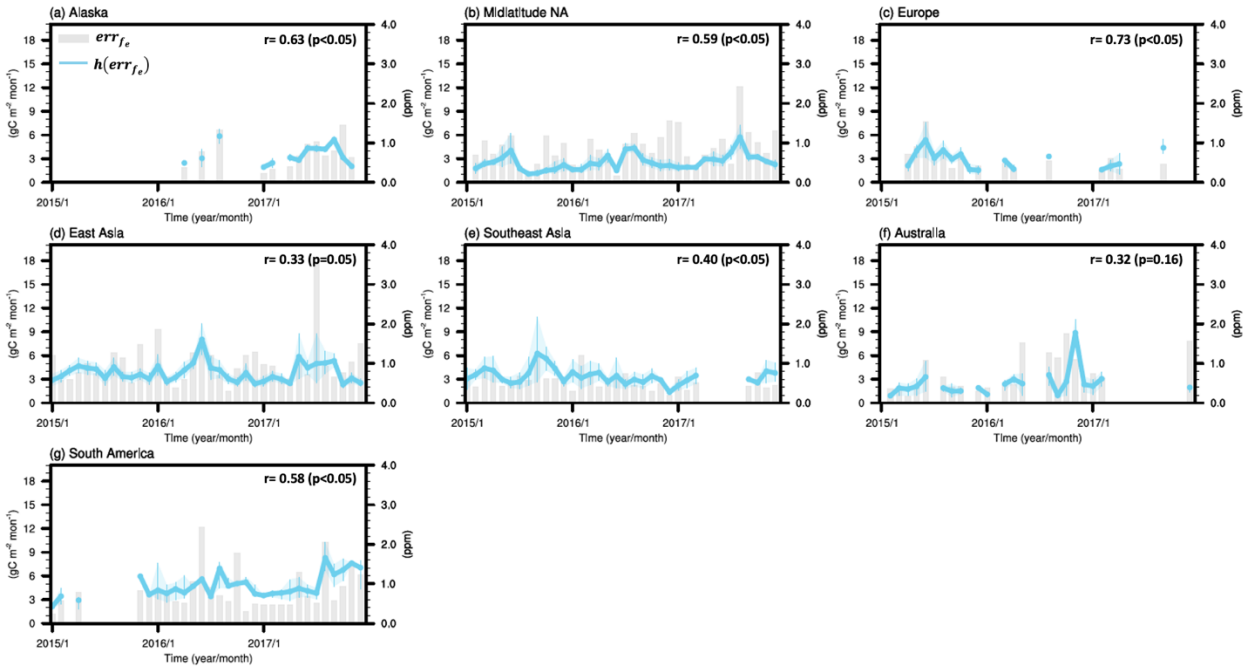

Figure S2. Monthly variations of $h(err_{f_e})$ (line) and err_{f_e} (bar) for each region. The upper right number indicates the correlation coefficient between them.

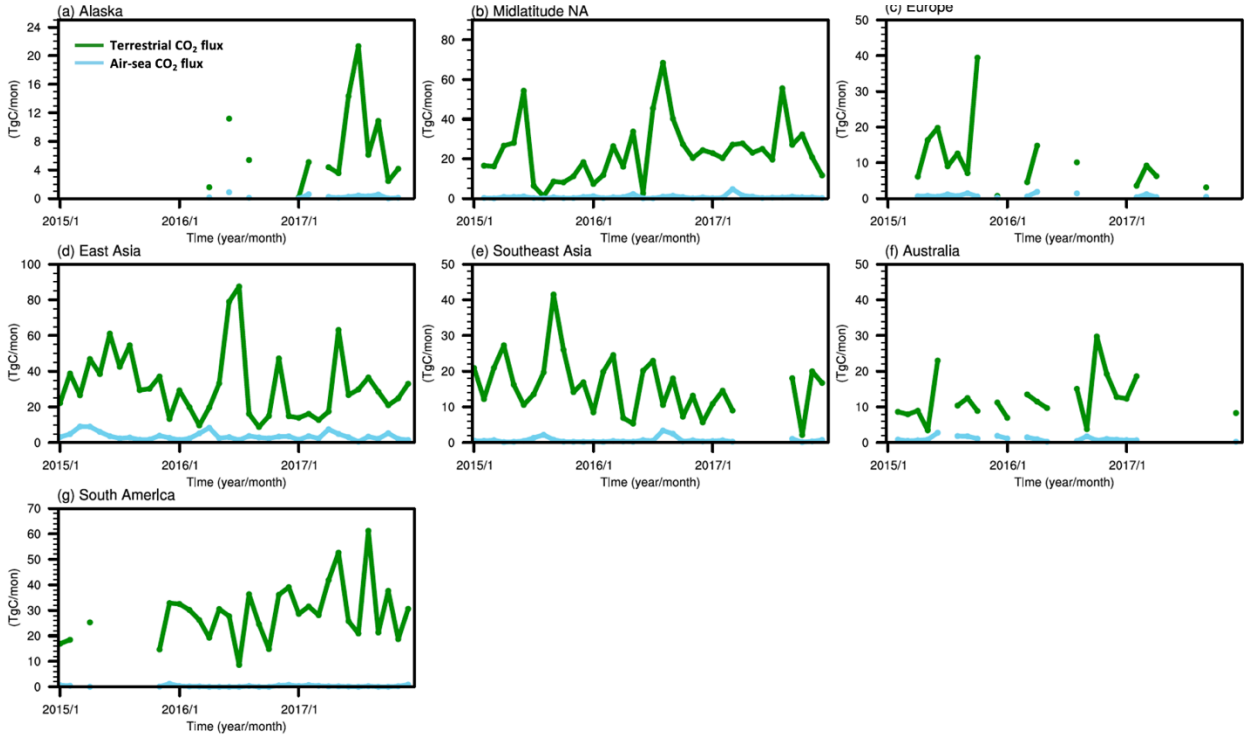

Figure S3. Monthly variations of one standard deviation of OCO-2 MIP inversion estimates in total land-atmosphere CO_2 fluxes (green line) and total ocean-atmosphere CO_2 fluxes (blue line) within the effective area to aircraft measurements for each region.

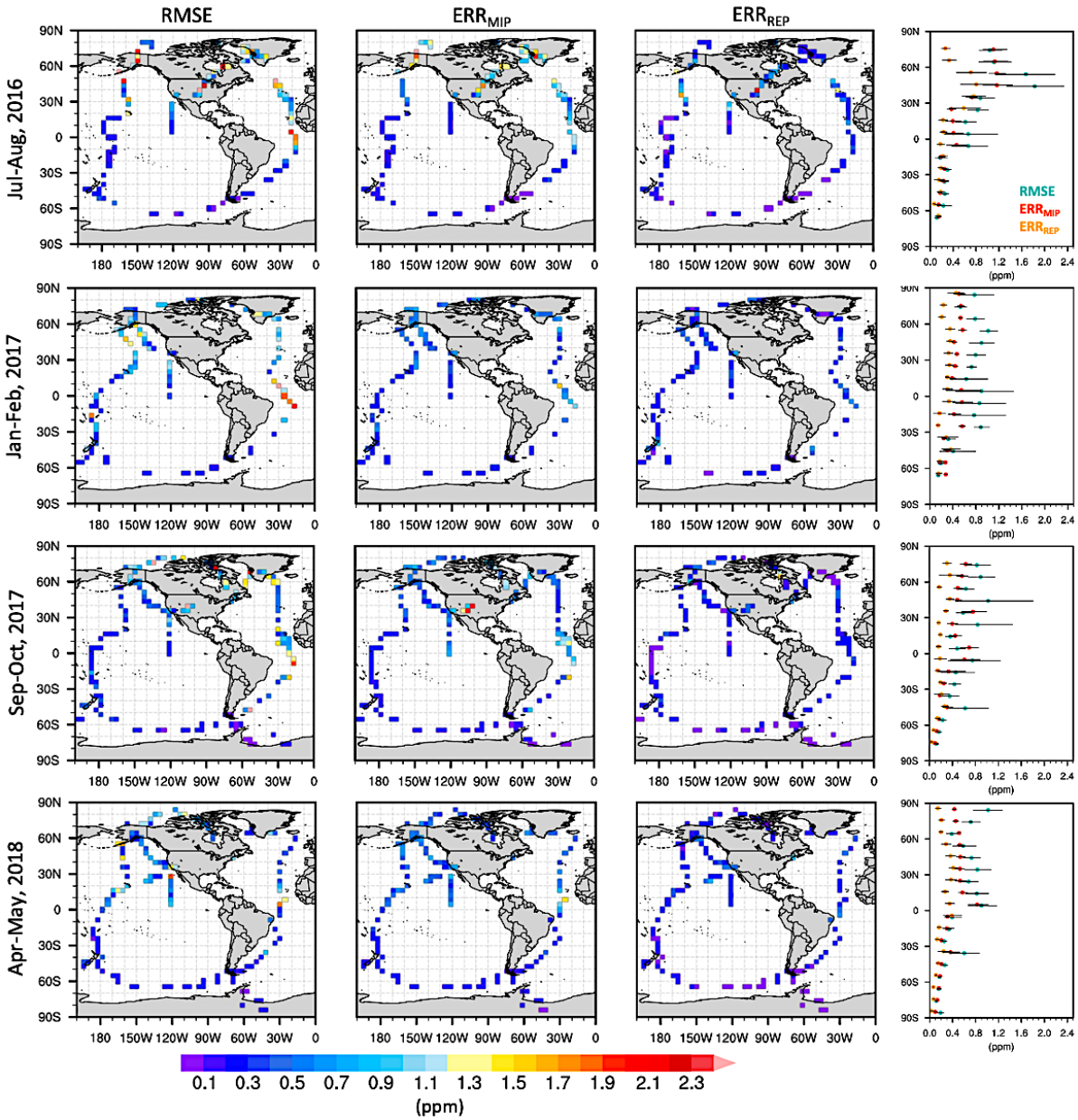

Figure S4. Spatial distributions of *RMSE, ERR$_{MIP}$*, and *ERR$_{REP}$* for each ATom campaign period. Right-hand panels show their latitudinal distributions smoothed by 10° moving average (dot) with 95% confidence intervals derived from 1000 bootstrap samples of datasets (error bar).

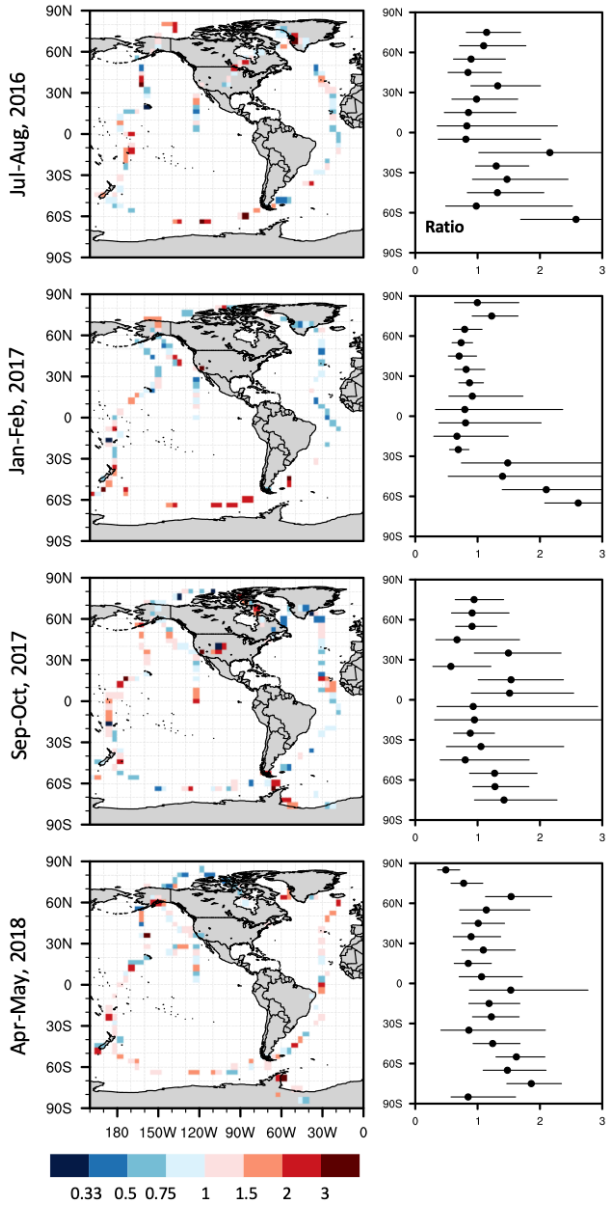

Figure S5. Same as Figure S4 but for Ratio.

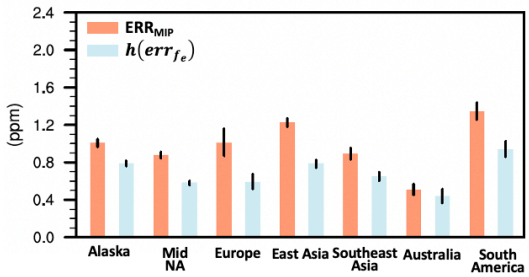

Figure S6. Regional mean values of ERR_{MIP} and $h(err_{f_e})$ for the period 2015–2017. The error bars represent the 95% confidence intervals derived from 1000 bootstrap samples of datasets.

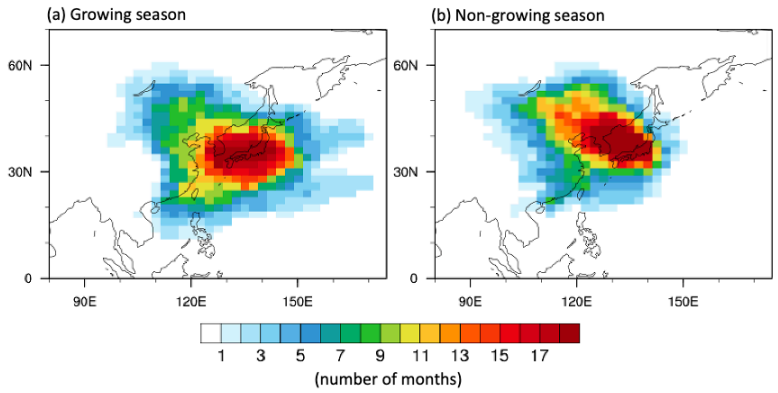

Figure S7. Number of months selected as the effective area for airborne measurements in East Asia during (a) the vegetation growing season and (b) the non-growing season for the period 2015–2017.

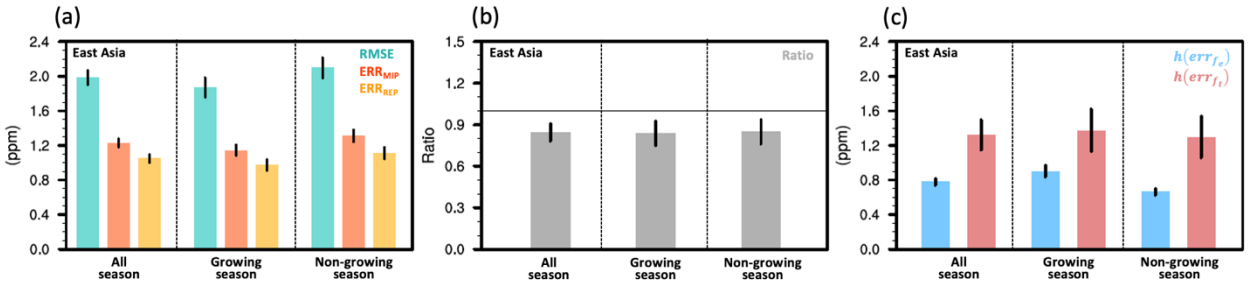

Figure S8. Mean values of monthly (a) *RMSE, ERR*$_{MIP}$*, ERR*$_{REP}$, (b) *Ratio*, (c) $h(err_{f_e})$, and $h(err_{f_t})$ in East Asia for each season for the period 2015–2017. The error bars represent the 95% confidence intervals derived from 1000 bootstrap samples of datasets.

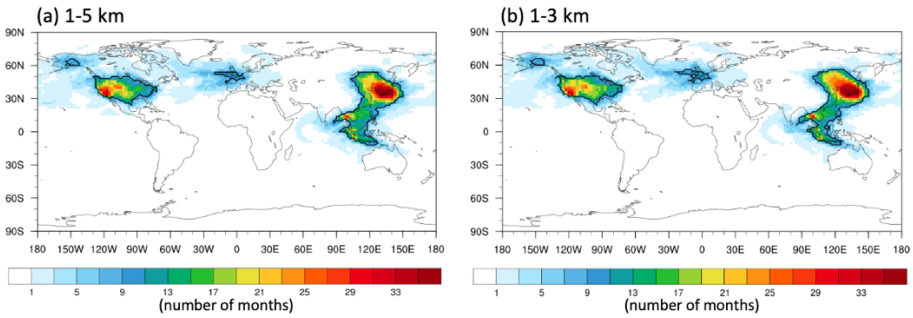

Figure S9. Number of months selected as the effective area for airborne measurements made within (a) the 1-5 km a.g.l. altitude range and (b) 1-3 km a.g.l. altitude range in Alaska, mid-latitude North America, Europe, East Asia, and Southeast Asia for the period 2015–2017. The outlined area represents selected areas for more than eight months or equal.

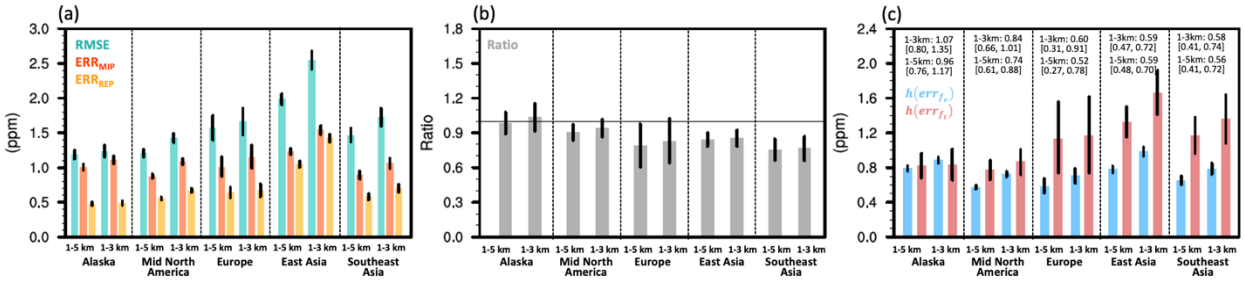

Figure S10. Mean values of monthly (a) *RMSE, ERR$_{MIP}$, ERR$_{REP}$*, (b) *Ratio*, (c) $h(err_{f_e})$, and $h(err_{f_t})$ derived from atmospheric CO_2 data within either the 1-5 km or 1-3 km a.g.l. altitude range for each region for the period 2015–2017. The numbers at the top of panel (c) indicate the ratio of the three-year mean $h(err_{f_e})$ to $h(err_{f_t})$. The error bars and error ranges represent the 95% confidence intervals derived from 1000 bootstrap samples of datasets.

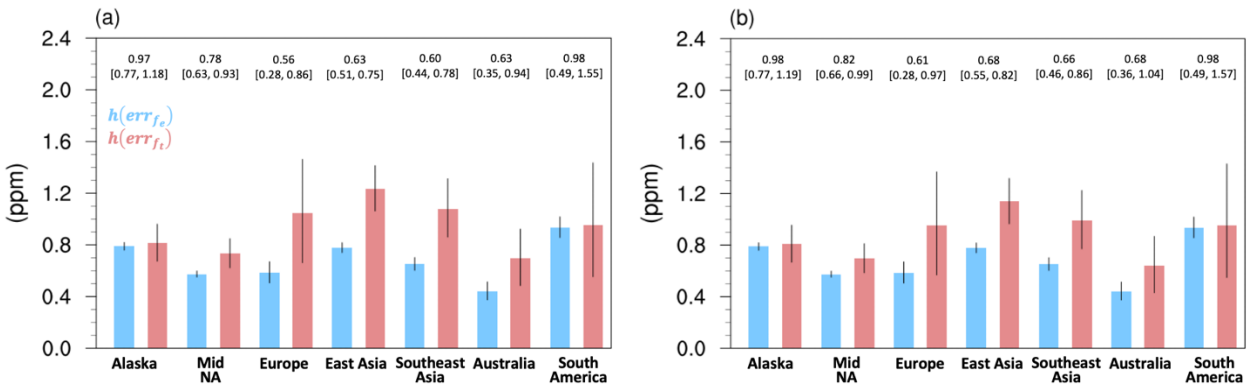

Figure S11. Mean values of monthly $h(err_{f_e})$, and $h(err_{f_t})$ for each region for the period 2015–2017 where (a) $h(err_{f_t})^2 - h(err_{f_e})^2 = 0.8 \cdot (RMSE^2 - ERR_{TOT}^2)$ and (b) $h(err_{f_t})^2 - h(err_{f_e})^2 = 0.6 \cdot (RMSE^2 - ERR_{TOT}^2)$. The numbers at the top of each panel indicate the ratio of the three-year mean $h(err_{f_e})$ to $h(err_{f_t})$. The error bars and error ranges represent the 95% confidence intervals derived from 1000 bootstrap samples of datasets.

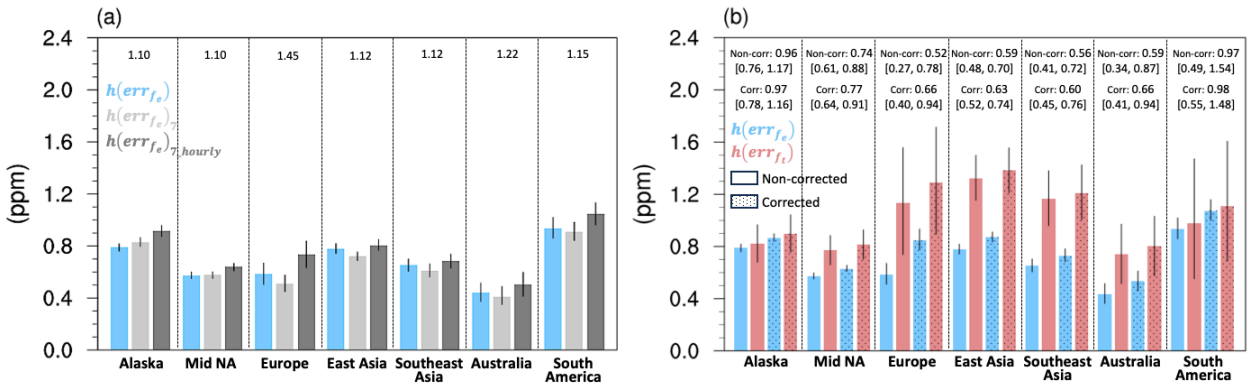

Figure S12. (a) Mean values of monthly $h(err_{f_e})$ for each region for the period 2015–2017, derived using different monthly posterior flux estimates from either 10 (blue) or 7 ($h(err_{f_e})_7$; light gray) OCO-2 MIP models with identical hourly NBE variation information, or from different monthly posterior flux estimates from 7 models with different hourly NBE variation information ($h(err_{f_e})_{7\_hourly}$; dark gray). The numbers at the top of the panel (a) indicate the ratio of $h(err_{f_e})_{7\_hourly}$ to $h(err_{f_e})_7$. **(b)** Mean monthly values of $h(err_{f_e})$ (blue) and $h(err_{f_t})$ (red) for each region over three years, with the dotted bars representing the corrected $h(err_{f_e})$, obtained by multiplying the ratio of $h(err_{f_e})_{7\_hourly}$ to $h(err_{f_e})_7$, and the recalculated $h(err_{f_t})$ using these corrected $h(err_{f_e})$ values. The numbers at the top of the panel (b) denote the ratio of $h(err_{f_e})$ to $h(err_{f_t})$. The error bars represent the 95% confidence intervals derived from 1000 bootstrap samples of datasets.